Available online at www.sciencedirect.com
SCIENCE DIRECT®
Journal of Catalysis 219 (2003) 389–403
JOURNAL OF CATALYSIS
www.elsevier.com/locate/jcat

# Production of hydrogen from methanol over Cu/ZnO catalysts promoted by $ZrO_2$ and $Al_2O_3$

J. Agrell,[a,*,1] H. Birgersson,[a] M. Boutonnet,[a] I. Melián-Cabrera,[b,2] R.M. Navarro,[b] and J.L.G. Fierro [b]

[a] *KTH–Royal Institute of Technology, Chemical Technology, SE-100 44 Stockholm, Sweden*
[b] *ICP–Instituto de Catálisis y Petroleoquímica, CSIC, Cantoblanco, 28049 Madrid, Spain*

Received 26 February 2003; revised 6 May 2003; accepted 6 May 2003

**Abstract**

Production of $H_2$ from methanol by steam reforming, partial oxidation, or a combination thereof was studied over Cu/ZnO-based catalysts. The catalysts were characterized by a variety of techniques, including $N_2O$ chemisorption, X-ray photoelectron spectroscopy, X-ray diffraction, and temperature-programmed reduction/oxidation. The influence of feed composition, reaction temperature, and catalyst formulation on $H_2$ production rate, product distribution, and catalyst lifetime was investigated. Distinct differences between the processes were observed with respect to catalyst behavior. $ZrO_2$-containing catalysts, especially $Cu/ZnO/ZrO_2/Al_2O_3$, exhibit the best performance in the steam reforming reaction. During partial oxidation, however, a binary Cu/ZnO catalyst exhibits the lowest light-off temperature and the lowest level of CO by-product. The redox properties of the catalyst appear to play a key role in determining the pathway for $H_2$ production. In particular, the extent of methanol and/or $H_2$ combustion at differential $O_2$ conversion is strongly dependent on the ease of copper oxidation in the catalyst.


*Keywords:* Fuel cell; Methanol steam reforming; Methanol oxidation (partial); $Cu/ZnO/ZrO_2/Al_2O_3$ catalyst; Characterization; $N_2O$ chemisorption; TPR/TPO; XPS

## 1. Introduction

Vehicles powered by proton-exchange membrane (PEM) fuel cells are approaching commercialization. Unlike internal combustion engines (ICEs), fuel cells are not limited by the thermal efficiency of the Carnot cycle. Hence, the fuel utilization is much more efficient than in conventional heat engines. Furthermore, fuel cells are silent during operation and have no moving parts, and the emissions of hazardous compounds to the atmosphere are low or even nonexisting [1,2].

The PEM fuel cell generally requires $H_2$ as fuel. There are various strategies for on-board storage of $H_2$ in the vehicle, e.g., as gas compressed, as liquid, or in $H_2$-storage materials, such as metal hydrides and carbon nanotubes. However, all these options require a dedicated filling station infrastructure and raise issues concerning safety and cost.

Current trends indicate that PEM fuel cell vehicles will use liquid fuels, at least in the early stages of commercialization. Methanol is a fuel, which is readily available and can be catalytically converted into a $H_2$-rich gas at moderate temperature (200–300 °C). Methanol has a high H/C ratio and no C–C bonds, hence minimizing the risk for coke formation. Moreover, as methanol can be produced from renewable sources, its reforming does not contribute to a net addition of $CO_2$ to the atmosphere.

A process for production of $H_2$ on board a vehicle must meet several criteria. For instance, it must be compact and energy efficient, respond to transient behavior, and produce a reformate with a high $H_2$ content and extremely low CO levels. CO is a fuel cell poison that deactivates the Pt-based catalyst at the anode already at concentrations exceeding a few parts per million [3].

* Corresponding author.
*E-mail address:* johan.agrell@alfalaval.com (J. Agrell).
[1] Present address: Alfa Laval Tumba AB, Separation Technology Development, SE-147 80 Tumba, Sweden.
[2] Present address: Delft University of Technology, DelftChemTech (R&CE Section), Julianalaan 136, 2628 BL Delft, The Netherlands.

0021-9517/$ – see front matter 
doi:10.1016/S0021-9517(03)00221-5

In essence, there are three processes available for production of $H_2$ from methanol with low CO levels on board the vehicle [4]: steam reforming of methanol (SRM), partial oxidation of methanol (POM), and a combination of these two reactions, termed combined reforming of methanol (CRM).

SRM is an efficient process that yields high $H_2$ concentrations:

$$CH_3OH(l) + H_2O(l) \rightarrow CO_2 + 3H_2, \quad \Delta H^0 = 131 \text{ kJ/mol}. \tag{1}$$

Being an endothermic reaction, surplus energy can be recycled, promoting the overall system efficiency. However, the process is slow and requires long residence times, leading to slow start-up and poor transient response. Moreover, it requires external heat exchange.

POM is an exothermic reaction, resulting in a fast process with rapid start-up and dynamic response:

$$CH_3OH(l) + 0.5O_2 \rightarrow CO_2 + 2H_2, \quad \Delta H^0 = -155 \text{ kJ/mol}. \tag{2}$$

The reactor can be made small and lightweight due to the absence of heat-exchanger parts. However, the $H_2$ yield is low and further decreases due to the loss of $H_2$ through combustion. Hence, combining the best features of both processing methods appears attractive:

$$CH_3OH + (1-2a)H_2O + aO_2 \rightarrow CO_2 + (3-2a)H_2 \quad (0 \leqslant a \leqslant 0.5). \tag{3}$$

By feeding a mixture of methanol, water, and air, close to autothermal conditions can be maintained in the fuel processor. The feed composition can also be varied to meet the fuel cell's requirements at any given time. Thus, the endothermic SRM process provides a high $H_2$ production capacity and promotes overall efficiency, while POM enables fast start-up and dynamic response, as well as compactness.

In the literature, copper-based catalysts have received considerable attention for production of $H_2$ by SRM [5–21]. Recent papers have discussed the POM reaction [22–24], as well as the combined process for production of $H_2$ [25–38]. The $Cu/ZnO/Al_2O_3$ catalyst, which is traditionally used for low-temperature gas-shift and methanol synthesis, has been widely used in these reactions.

SRM is the reverse of methanol synthesis from $CO_2$ and $H_2$. Therefore, it is reasonable to assume that the methanol synthesis catalyst shows high activity also in the reverse reaction. In the presence of $O_2$, however, another type of catalyst may be even more efficient. Velu et al. [27,31,36], who studied the SRM reaction with addition of $O_2$, found that $ZrO_2$-containing $Cu/ZnO/Al_2O_3$ catalysts are best suited for production of $H_2$ with ultralow CO levels. In the present study, the catalyst compositions were chosen in accordance with the findings in Refs. [18,27,31,36].

Fisher and Bell studied the reaction mechanism for methanol synthesis and decomposition over $Cu/ZrO_2$-based catalysts. They suggested that a synergy exists between copper and $ZrO_2$, in which all the major reaction intermediates are found on $ZrO_2$, while copper dissociates molecular $H_2$, which is provided by a spillover mechanism [39–41].

In the present work, a series of Cu/ZnO materials containing $ZrO_2$ and $Al_2O_3$ were prepared by decomposition of hydroxycarbonate precursors formed by carbonate coprecipitation of metal nitrates in aqueous solution. Microscale activity measurements were carried out, paying attention to the influence of catalyst formulation, feed composition, and reaction temperature on $H_2$ production rate, product distribution, and catalyst stability. Catalyst characterization included $N_2O$ chemisorption, X-ray photoelectron spectroscopy (XPS), X-ray diffraction (XRD), temperature-programmed reduction (TPR), and oxidation (TPO), $N_2$ adsorption–desorption (BET), and inductively coupled plasma atomic emission spectroscopy (ICP-AES).

## 2. Experimental methods

### 2.1. Catalyst preparation

A series of copper-based catalysts were derived from hydroxycarbonate precursors prepared by coprecipitation of metal nitrates in aqueous solution. The method is based on the one described by Alejo et al. [22]. The catalysts are summarized in Table 1.

In short, nitrate salts of the metals were dissolved in the desired ratios in distilled water. $Cu(NO_3)_2$, $Zn(NO_3)_2$, and $Al(NO_3)_3$ were all obtained from J.T. Baker. $ZrO(NO_3)_2$ was obtained from Alfa Aesar. The total metal concentration in the aqueous solution was 1.25 M. $Na_2CO_3$ (J.T. Baker) in a 0.25 M aqueous solution was then added under vigorous stirring under $N_2$ atmosphere, while maintaining the pH constant at around 9 and the temperature at 60 °C. The precipitates were aged for ∼ 2 h and then recovered by filtration, followed by thorough washing with distilled water at ambient temperature to remove all traces of sodium. Drying

Table 1
A summary of the catalysts and their physicochemical properties

| Catalyst | Formula | Composition (wt%) | | | | BET area | $Cu^0$ area | Cu dispersion |
|---|---|---|---|---|---|---|---|---|
| | | Cu | Zn | Zr | Al | ($m^2/g$) | ($m^2/g$) | (%) |
| CZ | Cu/ZnO | 43.8 | 56.2 | – | – | 48.6 | 20.8 | 9.6 |
| CZA | $Cu/ZnO/Al_2O_3$ | 39.4 | 51.1 | – | 9.5 | 91.9 | 22.2 | 11.3 |
| CZZ | $Cu/ZnO/ZrO_2$ | 32.3 | 39.5 | 28.2 | – | 81.8 | 15.5 | 13.2 |
| CZZA | $Cu/ZnO/ZrO_2/Al_2O_3$ | 30.9 | 50.2 | 14.1 | 4.8 | 116.2 | 23.3 | 23.2 |

was carried out in air at 110 °C for 12 h and the final calcination was performed in air at 350 °C for 12 h. The obtained powders were then milled and sieved and the fraction containing particles of 0.12–0.25 mm was used in the activity measurements.

The prepared catalysts are summarized in Table 1, where they are named according to their composition. For instance, catalyst CZZA contains CuO, ZnO, $ZrO_2$, and $Al_2O_3$.

### 2.2. Catalyst characterization

The catalysts were characterized using a variety of techniques, which are briefly outlined below.

#### 2.2.1. $N_2$ adsorption–desorption

The specific surface areas of the calcined samples were calculated from $N_2$ adsorption–desorption data acquired at liquid $N_2$ temperature on a Micromeritics ASAP 2010 instrument. The powders were first outgassed at 250 °C to ensure a clean surface prior to acquisition of the adsorption isotherm. A cross-sectional area of 0.164 $nm^2$ of the $N_2$ molecule was assumed in the calculations of the specific surface areas using the method of Brunauer, Emmet, and Teller (BET).

#### 2.2.2. Atomic emission spectroscopy

The chemical composition of the calcined catalysts was measured by inductively coupled plasma atomic emission spectroscopy, using a Perkin-Elmer Optima 3300DV instrument. The powders were first dissolved in acidic solutions (mixtures of $HNO_3$, HCl, and HF, as appropriate), microwaved for 15 min, and then diluted to concentrations within the detection range of the instrument.

#### 2.2.3. X-ray diffraction

Powder X-ray diffraction measurements provided information about crystalline phases and crystallite size in the catalysts. A Siemens D5000 instrument using monochromatic Cu-$K_\alpha$ radiation was employed, scanning $2\theta$ from 20 to 80°.

#### 2.2.4. X-ray photoelectron spectroscopy

X-ray photoelectron spectroscopy was used to study the chemical composition and oxidation state of catalyst surfaces. The XPS instrument, a VG Escalab 200 R spectrometer with a Mg-$K_\alpha$ X-ray source ($h\nu = 1253.6$ eV; 1 eV = $1.602\times10^{-19}$ J), was equipped with a pretreatment chamber with controlled atmosphere and temperature in which the catalyst samples could be exposed to different conditions. The catalyst was mounted on a sample rod, placed in the pretreatment chamber, and outgassed under vacuum prior to transferring to the analysis chamber. Subsequently, it was reduced in 400 mbar $H_2$ at 250 °C and again analyzed. Finally, the catalyst was exposed to a 1:2 mixture of $O_2$ and methanol at 250 °C and 60 mbar, and again inserted into the analysis chamber where measurements were carried out under vacuum.

The C1s, Cu2p, Zn2p, Al2p, and Zr3d core-level spectra were recorded and the corresponding binding energies were referenced to the C1s line at 284.9 eV (accuracy within ±0.1 eV). The $Cu_{LMM}$ and $Zn_{LMM}$ Auger peaks were also recorded and the modified Auger parameters ($\alpha_A$) calculated according to the equation below, where the expression in parentheses represents the difference between the kinetic energy of the Auger electron and the $2p_{3/2}$ photoelectron:

$$\alpha_A = h\nu + (\mathrm{KE}(M_{LMM}) - \mathrm{KE}(M2p_{3/2})) \quad (M = \mathrm{Cu}, \mathrm{Zn}). \tag{4}$$

#### 2.2.5. Temperature-programmed reduction/oxidation

Temperature-programmed reduction and oxidation experiments were carried out to study the copper dispersion and reducibility. Cycled TPR/TPO redox experiments gave additional information about the catalysts' resistance to sintering.

A TPD/TPR 2900 instrument from Micromeritics was used for the analyses. Approx 50 mg of a freshly calcined catalyst was placed on top of glass wool in a quartz reactor. In order to remove contaminants, the powder was pretreated in He flowing at 50 ml/min by elevating the temperature at 10 °C/min to 300 °C and keeping it isothermal for 30 min. After cooling to room temperature, TPR experiments were carried out in 10% $H_2$/Ar flowing at 90 ml/min, increasing the temperature at 10 °C/min. The temperature ramp was interrupted at 500 °C, after which the sample was cooled in $N_2$ to ambient temperature. The TCD current was maintained at 50 mA and the detector temperature at 100 °C. A cryogenic trap consisting of a gel formed by adding liquid $N_2$ to isopropanol in a thermos flask was used to prevent water from entering the detector.

Subsequent temperature-programmed reoxidation of the reduced samples was carried out in 3% $O_2$/He flowing at 110 ml/min, again ramping the temperature at 10 °C/min. The temperature was increased to 450 °C, which was maintained for 1 h to ensure complete oxidation. The TCD current was maintained at 75 mA and the detector temperature at 100 °C.

Finally, the samples were rereduced according to the TPR procedure described above.

#### 2.2.6. $N_2O$ chemisorption

The specific $Cu^0$ surface areas of the catalysts were measured by nitrous oxide ($N_2O$) chemisorption, using a method similar to the one described by Chinchen et al. [42]. The method is termed reactive frontal chromatography (RFC). It consists of carefully oxidizing the exposed $Cu^0$ surface of a prereduced Cu/ZnO catalyst by switching the feed from an inert $N_2$ stream to a reactive $N_2O/N_2$ mixture:

$$2Cu_{(s)} + N_2O \rightarrow Cu_2O_{(s)} + N_2. \tag{5}$$

By quantifying the amount of consumed $N_2O$, a measurement of the $Cu^0$ surface area can be obtained. The equip-

ment consisted of a custom-built reactor setup and sample amounts of 100–200 mg were used in the experiments. After prereducing the catalyst at 250 °C for 1 h in 10% $H_2/N_2$ (50 ml/min), it was exposed to a stream of $N_2$ (> 99.995%, N45, Air Liquide) at the same temperature for 1 h and then cooled to the chemisorption temperature (60 °C). The $N_2$ flow (30 ml/min) was then exchanged for a 3% $N_2O/N_2$ mixture (30 ml/min) by switching a four-way valve. The delayed $N_2O$ front, which is caused by the decomposition of $N_2O$ on the exposed $Cu^0$ surface, was monitored using a gas chromatograph (GC) equipped with a thermal conductivity detector (TCD).

The typical line shape, the so-called reactive frontal chromatogram, is not an ideal step. Because of this, a blank switch over the oxidized catalyst is necessary to use as reference for the calculation. Subtracting the curves and integrating over time gives the total amount of $N_2O$ consumed by surface copper atoms. The $Cu^0$ surface area was calculated assuming a molar stoichiometry of $N_2O/Cu_{(s)} = 0.5$, where $Cu_{(s)}$ denotes a superficial copper atom, and an average value of $1.46 \times 10^{19}$ copper atoms/$m^2$ for the surface density of copper metal [43].

### 2.3. Catalytic activity measurements

Catalytic experiments were performed at atmospheric pressure in a packed-bed microreactor consisting of a quartz tube with an internal diameter of 6 mm and a coaxially centered thermocouple with its tip located in the middle of the bed. The catalyst was diluted to avoid adverse thermal effects. Both catalyst and diluent were sieved to in order minimize the pressure drop over the bed, which rested on a porous quartz disc. The methanol or methanol/water mixture was fed to the evaporator by means of a liquid syringe pump. For the oxidation reactions, air was added by means of a Brooks 5850 mass flow controller.

The reaction conditions are described in Table 2. One set of experiments was carried out under slightly different conditions (POM/2), but on a similar reactor setup. It is indicated in the text when these conditions were used.

Table 2
Experimental conditions for catalytic activity measurements (gas flow rates given at 20 °C and 1 atm)

| | SRM | CRM | POM/1 | POM/2 |
|---|---|---|---|---|
| Catalyst load (mg) | 50[a] | 50[a] | 50[a] | 100[b] |
| Particle size (mm) | 0.12–0.25 | 0.12–0.25 | 0.12–0.25 | 0.25–0.5 |
| Pressure | Atmospheric | Atmospheric | Atmospheric | Atmospheric |
| $H_2O/CH_3OH$ (M) | 1.3 | 1.3 | – | – |
| $O_2/CH_3OH$ (M) | – | 0.2 | 0.2 | 0.25 |
| Methanol (ml/h) | 1.3 | 1.3 | 1.3 | 1.1 |
| Water (ml/h) | 0.7 | 0.7 | – | – |
| Air (ml/min) | – | 14 | 14 | 14 |
| Total flow (ml/min) | 230[c] | 230[c] | 230[c] | 25 |

POM/1 reaction conditions were used for the partial oxidation experiments, unless otherwise noted in the text.
[a] Diluted with $SiO_2$ (quartz, nonporous) to 500 mg.
[b] Diluted 2:1 (vol) with SiC (nonporous).
[c] Diluted with $N_2$, as required.

Prior to each experiment, the catalyst was reduced in situ at 250–300 °C in a stream of 10% $H_2/N_2$. The catalysts containing $Al_2O_3$ and/or $ZrO_2$ were reduced at the higher temperature. The dwell time was at least 1 h in all cases.

Some catalysts were calcined again after reaction in order to study the effect of sintering on activity. This was also done in situ by flowing 6% $O_2/N_2$ at 50 ml/min and heating at 10 °C/min to 425 °C. These catalysts were then reduced again and their activity measured.

The product gas composition was analyzed on-line by a Varian gas chromatograph. The GC was equipped with a thermal conductivity detector and two packed columns in series (one for separation of polar components, i.e., $CO_2$, water, methanol, formaldehyde, methyl formate, and DME, and a molecular sieve for separation of $H_2$, $O_2$, $N_2$, and CO). He was used as the carrier gas.

In the following text, the product gas composition refers to the composition of the gas stream leaving the reactor, including unconverted methanol and $O_2$, but excluding $N_2$ used for dilution.

## 3. Results and discussion

The results from catalyst characterization are summarized in Table 1 and in the following text.

### 3.1. BET surface area

The binary CZ catalyst possesses the lowest BET surface area of all (49 $m^2/g$), as expected. By addition of either $ZrO_2$ or $Al_2O_3$, both structural promoters, the surface area increases to 82 and 92 $m^2/g$, respectively. The quaternary catalyst, CZZA, displays the highest surface area (116 $m^2/g$). It should be noted that the amount of additive varies in the catalysts. While CZA contains only 10 wt% aluminum, CZZ contains almost 30 wt% zirconium (as metal). The compositions were chosen in agreement with the recommendations by Velu et al. [27,31,36], who found that these formulations gave the best enhancement of catalyst activity.

### 3.2. Copper dispersion

$N_2O$ chemisorption experiments enabled measurements of the catalysts' $Cu^0$ surface areas. These varied from 15.5 to 23.3 $m^2/g$ (Table 1), catalyst CZZA exhibiting the highest value. As the catalysts contain different amounts of copper, 30 to 45 wt%, and the chemical compositions of the catalysts were known from ICP-AES measurements, the copper dispersions were calculated. They range from 9.6 to 23.2%, catalyst CZZA again exhibiting the highest value. It is clear that addition of $Al_2O_3$ or $ZrO_2$, both high-surface-area metal oxides, provides a larger surface on which copper can be dispersed. Clearly a combination of the two constitutes the

most favorable option. This is consistent with the findings of Velu et al. [31,36], who demonstrated that substitution of aluminum for zirconium improves copper dispersion, as well as reducibility. CZ exhibits the lowest copper dispersion, as expected in absence of a structural stabilizer.

### 3.3. Crystalline structure

The X-ray diffractograms of all four catalysts after calcination are shown in Fig. 1. The pattern of CZ after exposure to POM/1 reaction conditions is also inserted. This catalyst was diluted with $SiO_2$ to 10 wt% prior to reaction. That is why the intensity has been multiplied by a factor 10, also explaining the noise in the signal. The characteristic peaks of CuO and ZnO have been indicated in the diffractogram of CZ after calcination. No other features are observed, except in CZ after exposure to reaction conditions, in which the characteristic line of $Cu^0$ appears at $2\theta \approx 43°$. In this catalyst, the features associated with CuO are no longer observed.

Signals from crystalline zirconium and aluminum oxide phases would be expected in the ternary and quaternary materials, in addition to CuO and ZnO. However, in CZZ and CZZA, only features associated with ZnO are detected. This indicates that CuO is highly dispersed, which is in full agreement with the $N_2O$ chemisorption experiments. This is due to the fact that zirconium and aluminum are present in highly disordered or amorphous states because of the relatively low calcination temperature (350 °C), or that the crystallite size is too small to be detected due to line-broadening. Moreover, these elements are present in small quantities, their contents ranging from 5 to 30 wt% (as metals).

In CZA, on the other hand, the characteristic CuO lines exhibit high intensities, indicating relatively large crystallites. The ZnO crystals, however, appear to be small (line-broadening).

### 3.4. Temperature-programmed reduction

The TPR profiles of the freshly calcined and reoxidized catalysts are shown in Fig. 2. The profiles correspond to reduction of CuO

$$CuO + H_2 \rightarrow Cu^0 + H_2O. \quad (6)$$

The TPR profile of the CZ sample consists of at least three overlapping peaks. The onset of reduction is apparent at 135 °C. At around 180 °C, $H_2$ consumption increases rapidly, reaching a maximum at 190 °C. There is a shoulder at 200 °C and reduction is complete at about 225 °C. Subsequent oxidation and rereduction increases the particle size and the temperature needed for complete reduction to approximately 290 °C. The redox treatment homogenizes the

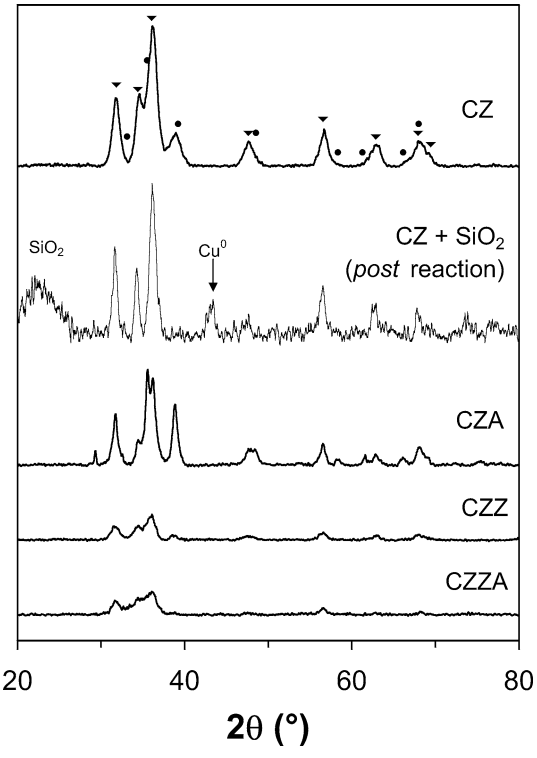


Fig. 1. X-ray diffractograms of the calcined catalysts and of catalyst CZ (diluted to 10 wt% with $SiO_2$) after exposure to reaction conditions ((●) CuO; (▼) ZnO).

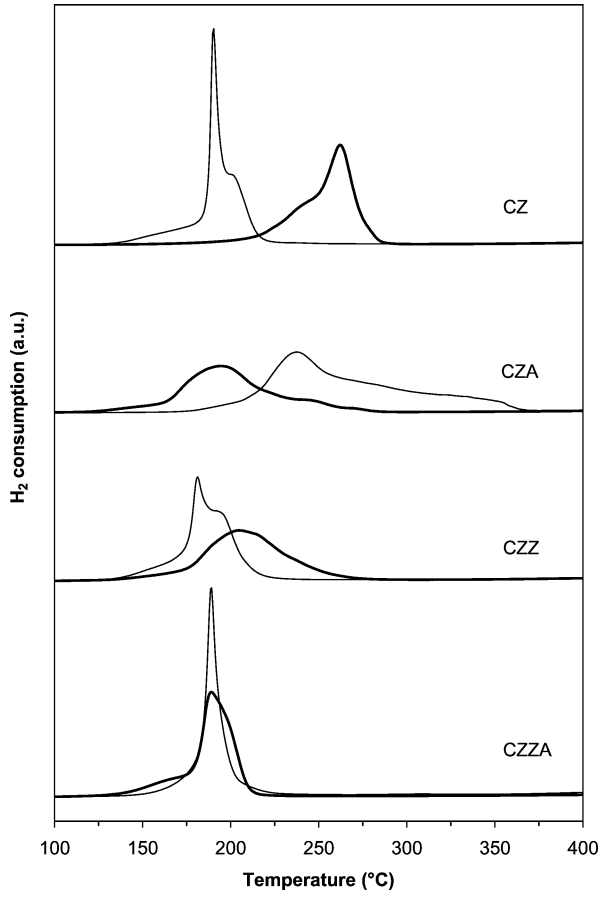


Fig. 2. Temperature-programmed reduction profiles of the freshly calcined (thin lines) and reoxidized (thick lines) catalysts.

material by sintering the most reactive small copper particles, decreasing the peak width at the base and making the profile more symmetrical.

The freshly calcined CZA catalyst requires a surprisingly high temperature for complete reduction. The main peak is located at 238 °C, with a long tail extending to temperatures as high as 370 °C. This indicates large CuO crystallites and/or possibly a strong interaction between copper and support. In the XRD measurements, high intensities were observed for the peaks associated with CuO, indicating large crystallites. After reoxidation, the peak maximum is unexpectedly shifted toward lower temperatures (195 °C) and the tail is diminished. In other words, the redox treatment appears to improve the dispersion of copper in the catalyst. A possible restructuring of the aluminum component could be the explanation for this observation.

The reduction profile of the fresh CZZ catalyst is similar to that of CZ, with three overlapping peaks distinguishable. The onset of reduction is observed at 135 °C, and the slope increases rapidly at about 170 °C, reaching a maximum at 182 °C. A shoulder is visible at 195 °C and reduction is complete at about 230 °C. After reoxidation, the profile is more symmetrical, displaying a peak at 208 °C, and reduction is complete at around 275 °C.

CZZA displays the lowest reduction temperature, both before and after reoxidation, the main peak appearing at approximately 190 °C. This indicates small CuO particles and hence, a high dispersion. These results correlate well with the $Cu^0$ surface area measurements, where the highest dispersion was found in this catalyst. Likewise, there is good correlation with the XRD measurements, which evidenced a small CuO particle size in this material. The reduction profile is narrow and almost symmetrical, both before and after reoxidation, indicating a narrow particle size distribution and a material of homogeneous composition. The temperature of the peak is comparable to that of catalyst CZ *before* reoxidation. In the case of CZZA, however, small particles and a narrow size distribution is retained after reoxidation.

It should be noted that the TPR measurement cannot be explained only in terms of copper dispersion. When the results are compared to the XRD and $N_2O$ chemisorption measurements, it is clear that factors other than dispersion, e.g., CuO crystallinity and interactions between the copper and the oxide support, influence the reducibility of the catalytic materials.

As large crystallites tend to be reduced more slowly than small ones due to their relatively lower surface area exposed to $H_2$, sintering of copper may have been expected in catalysts CZZ and CZZA due to the presence of small, hence reactive, particles. However, it appears as if $ZrO_2$ and $ZrO_2/Al_2O_3$ effectively stabilize copper and prevent crystallite growth. As shown in Fig. 2, it is clear that all three stabilized catalysts (CZA, CZZ, and CZZA) exhibit better resistance to Cu/CuO particle growth upon successive TPR/TPO than the binary CZ catalyst.

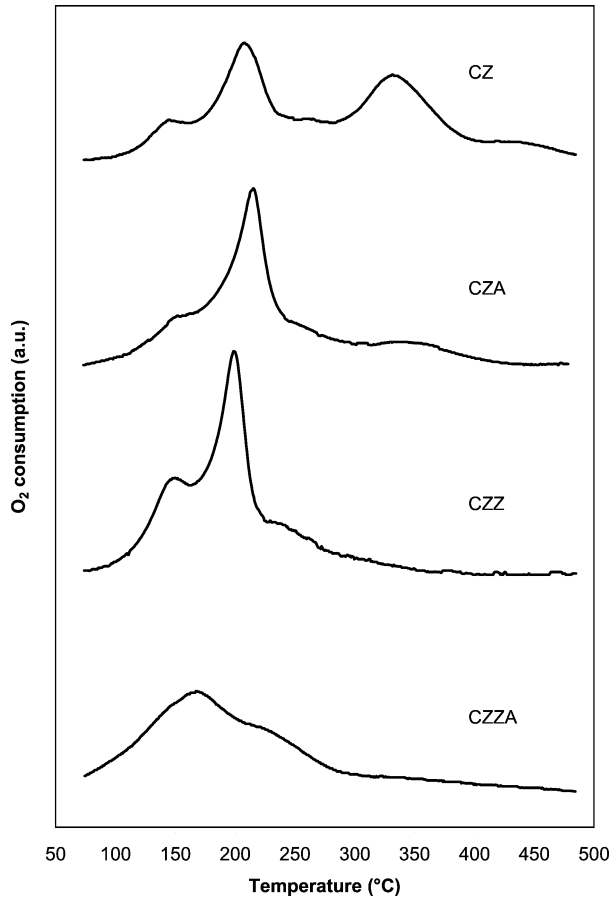


Fig. 3. Temperature-programmed oxidation profiles of the reduced catalysts.

### 3.5. Temperature-programmed oxidation

Fig. 3 shows the results from temperature-programmed oxidation of the four samples, which were previously reduced by TPR. $Cu^0 \rightarrow Cu^{2+}$ transformation takes place in all catalysts within the 75–450 °C temperature range. The profiles are complex and contain up to three peaks.

Catalysts CZ, CZA, and CZZ all display a shoulder or peak at about 150 °C and the main peak appears between 200 and 220 °C. CZ exhibits a second peak at 335 °C, while CZA and CZZ have long tails extending to higher temperatures. Catalyst CZZA displays just one peak at about 170 °C and a shoulder around 235 °C, oxidation being complete at 295 °C. The other catalysts require significantly higher temperatures for complete oxidation, up to ∼ 410 °C for catalyst CZ.

Li and Inui [44] studied the TPO profiles of reduced $Cu/ZnO/Al_2O_3$ catalysts prepared by carbonate coprecipitation of metal nitrates. These authors observed two or three oxidation peaks, which were ascribed to the stepwise oxidation of $Cu^0$. The low-temperature peak, located in the 150–200 °C region, was assigned to oxidation of $Cu^0$ to $Cu^+$ and the high-temperature peak (250–300 °C) to oxidation of $Cu^+$ to $Cu^{2+}$. An intermediate peak, which was

observed for some of the catalysts, was believed to span the transformation of $Cu^0$ in a hard oxidized state to $Cu^+$ and $Cu^+$ in an easily oxidized state to $Cu^{2+}$. Preceding work by Okamoto et al. [45] suggests that the hard oxidized state consists of crystalline copper, while the easily oxidized state corresponds to amorphous copper.

In agreement with these previous studies [44,45], we assign the two main peaks of catalyst CZ to the stepwise oxidation of $Cu^0$ ($Cu^0 \rightarrow Cu^+ \rightarrow Cu^{2+}$). In the present work, these peaks are shifted approx 50 °C toward higher temperatures, indicating a larger copper particle size, which is expected in the absence of a structural promoter. The intermediate peak/shoulder distinguishable at ∼ 270 °C may be ascribed to the transition via amorphous copper. However, the peak preceding the peak at ∼ 200 °C is not readily assigned.

When all the catalysts are compared, it is clear that the structurally stabilized catalysts, especially those containing $ZrO_2$, are more easily oxidized at low temperatures, indicating a high copper dispersion. In CZZA, copper oxidation appears to occur almost in a single step. This feature is important to bear in mind when investigating the catalysts' activity for methanol conversion in the presence of $O_2$.

### 3.6. Catalyst activity

The activity measurements were conducted in the same sequence for all catalysts, gradually increasing the heat of reaction. Hence, the SRM reaction was tested first, based on its endothermic nature. Secondly, CRM was carried out under close to autothermal conditions. Finally, the highly exothermic POM reaction was evaluated. By following this procedure, the catalysts were exposed to the same conditions and the comparison of results is relevant. The catalysts were reduced in $H_2/N_2$ prior to every set of experiments.

The SRM experiments were conducted with steam in excess of stoichiometry ($H_2O/CH_3OH = 1.3$), ensuring complete methanol conversion and suppressing CO formation by the reverse water–gas shift (RWGS) reaction:

$$CO_2 + H_2 \rightarrow H_2O + CO. \quad (7)$$

The $O_2$ pressure was maintained substoichiometric ($O_2/CH_3OH = 0.2$), as it has been shown that the loss of methanol and/or $H_2$ by combustion during POM is substantial under stoichiometric conditions ($O_2/CH_3OH = 0.5$) [22,24]:

$$CH_3OH + 1.5O_2 \rightarrow CO_2 + 2H_2O, \quad (8)$$

$$H_2 + 0.5O_2 \rightarrow H_2O. \quad (9)$$

The CRM reaction was studied under the same conditions as SRM and POM.

#### 3.6.1. Steam reforming of methanol

Fig. 4 shows a typical set of results for SRM over the CZ catalyst. As shown, the methanol conversion exhibits a typical S-shaped temperature dependence. $H_2$ and $CO_2$ are produced approx in a 3:1 ratio and CO formation is initiated at around 300 °C, when methanol conversion approaches completeness.

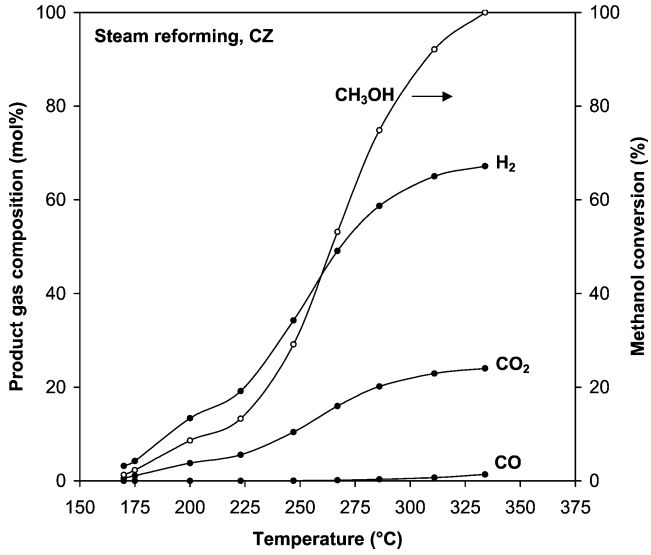


Fig. 4. Product gas composition and methanol conversion vs reaction temperature during steam reforming of methanol over catalyst CZ ($H_2O/CH_3OH = 1.3$ M).

The temperature at which complete conversion is obtained can be significantly lowered by decreasing the space velocity, as demonstrated in a previous paper from our laboratory [5]. However, an optimization with respect to this parameter was not the objective of the present study.

The behavior of all four catalysts is similar, the major differences being the temperature at which complete conversion is reached and the level of CO in the reformed gas. The temperatures required to reach 10, 50, and 90% methanol conversion ($T_{10}$, $T_{50}$, and $T_{90}$) over all four catalysts are given in Fig. 5. As shown, the temperatures are consistently lower for the materials containing $ZrO_2$ and $Al_2O_3$. This is due to the higher copper dispersion in these materials. Especially catalyst CZZA is very efficient in the SRM reaction. The corresponding CO levels (at $T_{10}$, $T_{50}$, and $T_{90}$) are shown in Fig. 6.

#### 3.6.2. Partial oxidation of methanol

POM results obtained over catalyst CZ are exemplified in Fig. 7. Being an exothermic reaction, ignition is rapid and thermal runaway is unavoidable in the low-temperature regime, although the reaction mixture is diluted with $N_2$ and the space velocity is maintained high. The methanol conversion only reaches about 40% at 325 °C as the $O_2$ pressure is maintained below stoichiometry. The situation is very similar over catalysts CZA, CZZ, and CZZA.

As shown, $H_2$ and $CO_2$ are produced approx in a 2:1 ratio in this reaction. Water is formed at low methanol conversions, but the water content decreases with increasing temperature as it is consumed by SRM. The vertical arrow in Fig. 7 indicates the temperature at which all $O_2$ has been

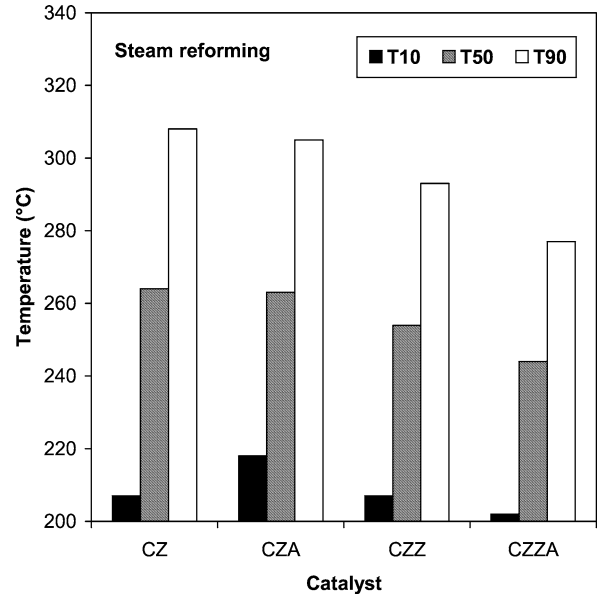


Fig. 5. The temperature required for 10, 50, and 90% conversion of methanol ($T_{10}$, $T_{50}$, and $T_{90}$) during steam reforming over catalysts CZ, CZA, CZZ, and CZZA ($H_2O/CH_3OH = 1.3$ M).

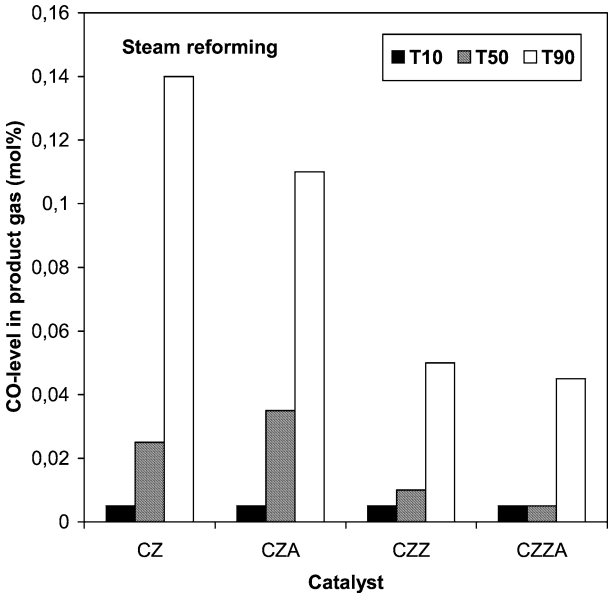


Fig. 6. The CO level in the product gas at 10, 50, and 90% methanol conversion during steam reforming of methanol over catalysts CZ, CZA, CZZ, and CZZA ($H_2O/CH_3OH = 1.3$ M).

consumed. At this point, water formation levels out and CO production is initiated. CO levels become more significant at higher temperatures as methanol decomposition increases in significance, producing CO as a primary product:

$$CH_3OH \rightarrow CO + 2H_2. \quad (10)$$

### 3.6.3. Combined reforming of methanol

The combination of SRM and POM was also investigated, termed combined reforming of methanol. The molar ratios of $O_2/CH_3OH$ and $H_2O/CH_3OH$ in the feed were

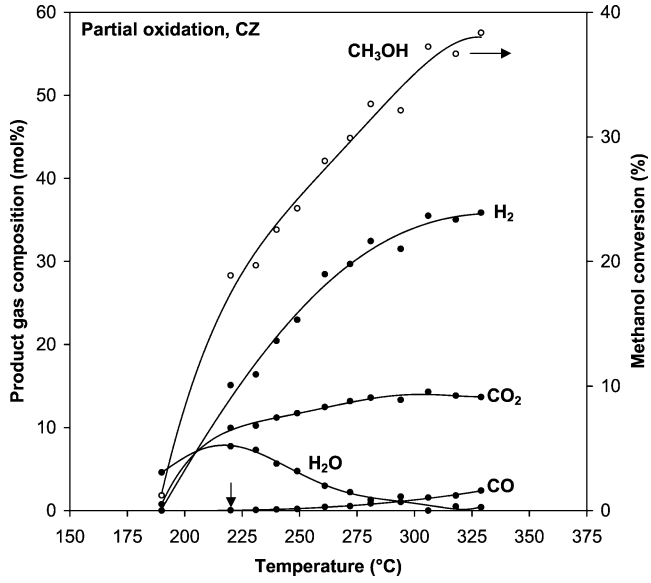


Fig. 7. Product gas composition and methanol conversion vs reaction temperature during partial oxidation of methanol over catalyst CZ ($O_2/CH_3OH = 0.2$ M). The vertical arrow indicates the point at which all $O_2$ has been converted.

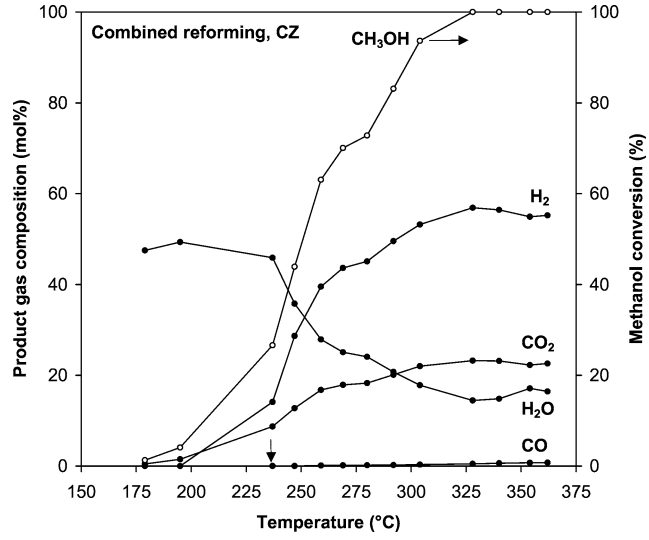


Fig. 8. Product gas composition and methanol conversion vs reaction temperature during combined reforming of methanol over catalyst CZ ($H_2O/CH_3OH = 1.3$; $O_2/CH_3OH = 0.2$ M). The vertical arrow indicates the point at which all $O_2$ has been converted.

maintained at 0.2 and 1.3, respectively. Fig. 8 shows a series of results over catalyst CZ.

In contrast to SRM and POM, water is both a reactant and a product in this process. At differential $O_2$ conversions, water is produced by combustion of methanol. When all $O_2$ has been converted (indicated by the vertical arrow in Fig. 8), water production levels off and $H_2$ formation is initiated.

During SRM, the $ZrO_2$-containing materials were consistently more active than the other catalysts. This is not the case during CRM. $T_{10}$, $T_{50}$, and $T_{90}$ for all four catalysts during CRM are given in Fig. 9. The $ZrO_2$-containing cata-

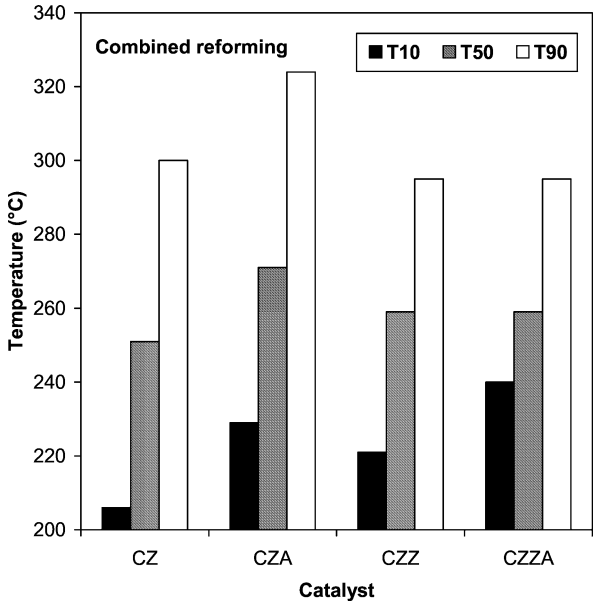


Fig. 9. The temperature required for 10, 50, and 90% conversion of methanol ($T_{10}$, $T_{50}$, and $T_{90}$) during combined reforming over catalysts CZ, CZA, CZZ, and CZZA ($H_2O/CH_3OH = 1.3$; $O_2/CH_3OH = 0.2$ M).

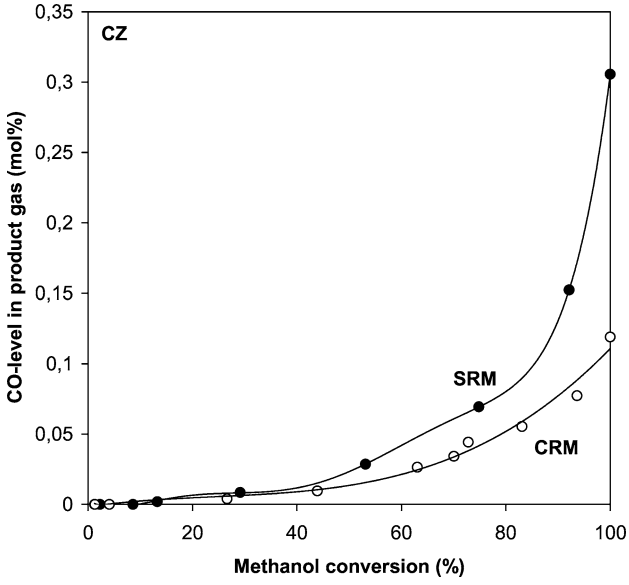


Fig. 10. CO level in the product gas vs methanol conversion during (●) steam reforming and (○) combined reforming of methanol over catalyst CZ ($H_2O/CH_3OH = 1.3$; $O_2/CH_3OH = 0.2$ M).

lysts still perform well at high methanol conversion, but the binary CZ catalyst is more efficient at low conversions.

CO production begins at high methanol conversions during CRM (cf. SRM). In Fig. 10, the CO level over catalyst CZ has been plotted vs methanol conversion during CRM and SRM. It is clear that CO formation over this catalyst is less pronounced during CRM than in the SRM reaction. The difference is not as pronounced over the other catalysts, which exhibit low CO levels throughout.

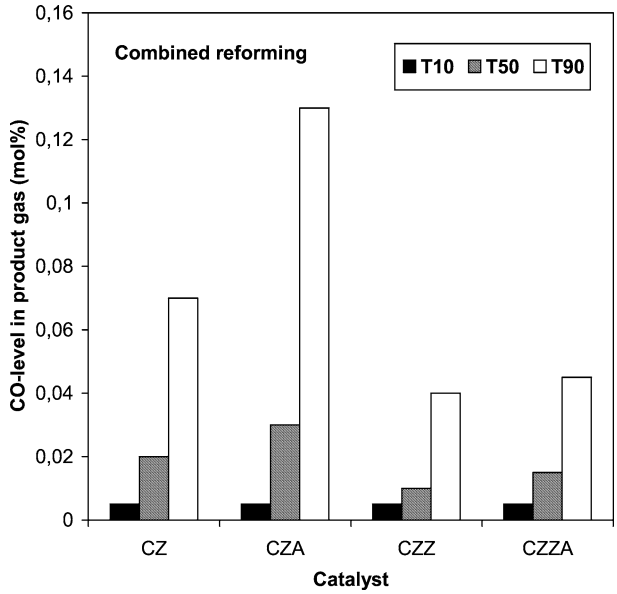


Fig. 11. The CO level in the product gas at 10, 50, and 90% conversion of methanol during combined reforming over catalysts CZ, CZA, CZZ, and CZZA ($H_2O/CH_3OH = 1.3$; $O_2/CH_3OH = 0.2$ M).

The CO levels at $T_{10}$, $T_{50}$, and $T_{90}$ for all the catalysts during CRM are shown in Fig. 11. Clearly, $ZrO_2$ suppresses CO formation, as during SRM. Some contribution from direct oxidation of CO can be expected in the presence of $O_2$:

$$CO + 0.5O_2 \rightarrow CO_2. \quad (11)$$

Additionally, as water is produced by combustion of methanol and/or $H_2$, the increased water content in the gas mixture can be expected to promote water–gas shift:

$$H_2O + CO \rightarrow CO_2 + H_2. \quad (12)$$

### *3.6.4. Catalyst stability*

Copper has a low Hüttig temperature [46], reflected by its relatively low melting point (1083 °C). It is well known that $Cu/ZnO/Al_2O_3$ catalysts suffer thermal deactivation at temperatures exceeding 300–350 °C [47]. Therefore, some measures were taken in order to prevent deactivation of the catalysts in the present study. For instance, the catalysts were diluted with $SiO_2$, the feed was diluted with $N_2$, the space velocity was maintained high, and the reaction temperature was kept below 350 °C. However, hot spots may still appear in the bed and care must be taken when operating the catalysts under exothermic conditions.

The performance of catalysts CZ and CZZA during extended on-stream operation was investigated in the CRM reaction at 260 °C. The temperature was chosen such that the conversion of methanol was in the range where the heat of reaction reaches its highest value. The results are shown in Fig. 12. Clearly, $ZrO_2$ doping greatly improves the lifetime of the catalyst. However, it should be noted that the reproduction of these results was not attempted.

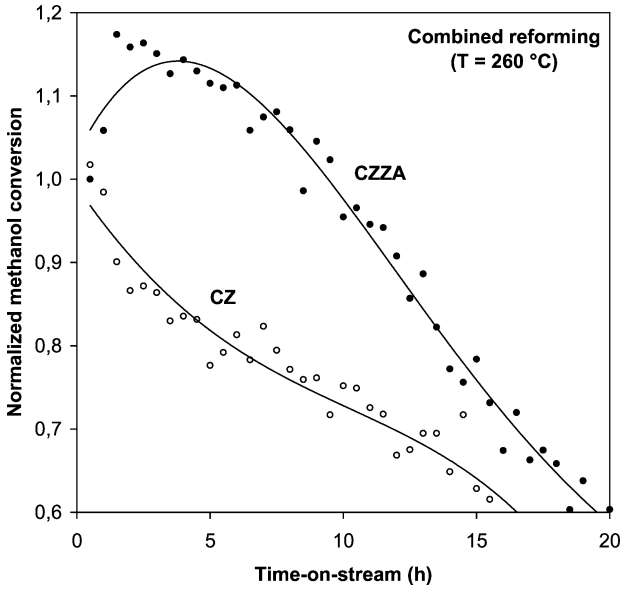


Fig. 12. Normalized methanol conversion vs time on stream during combined reforming of methanol at 260 °C over catalysts (○) CZ and (●) CZZA ($H_2O/CH_3OH = 1.3$; $O_2/CH_3OH = 0.2$ M).

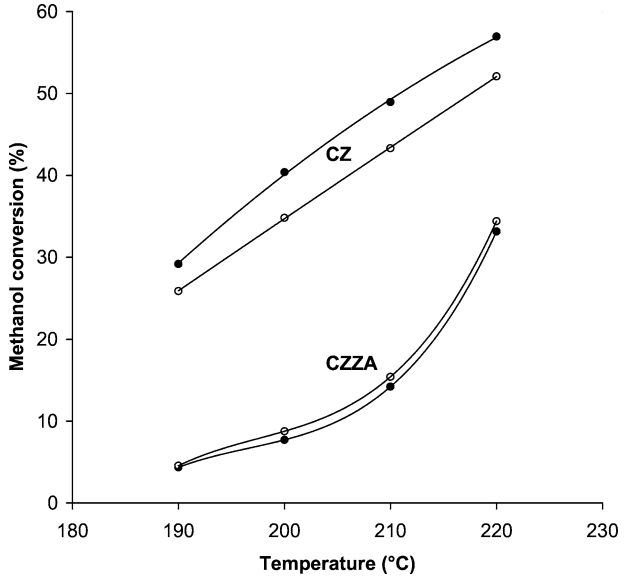


Fig. 13. Methanol conversion vs temperature in the POM reaction ($O_2/CH_3OH = 0.25$ M) over catalysts CZ and CZZA (●) before and (○) after a second calcination at 425 °C. POM/2 reaction conditions were used (cf. Table 2).

### 3.6.5. Catalyst activity after reduction–oxidation cycles

The POM activity of catalysts CZ and CZZA after a second calcination at 425 °C was also investigated. The results are shown in Fig. 13 and Table 3. It is clear that the performance of CZ deteriorates as a result of the oxidative treatment. This is in full agreement with the TPR-TPO results, where this material exhibited significant copper crystallite growth upon redox cycles (as described in the experimental section).

Table 3
Partial oxidation activity measurements ($O_2/CH_3OH = 0.25$ M) over catalysts CZ and CZZA before and after reoxidation at 425 °C (6% $O_2/N_2$)

| Catalyst | Temperature (°C) | Methanol conversion (%) | | Ratio |
|---|---|---|---|---|
| | | Fresh catalyst | Reoxidized catalyst | |
| CZ | 190 | 29.2 | 25.9 | 0.89 |
| | 200 | 40.4 | 34.8 | 0.86 |
| | 210 | 49.0 | 43.3 | 0.88 |
| | 220 | 57.0 | 52.1 | 0.91 |
| CZZA | 190 | 4.4 | 4.6 | 1.05 |
| | 200 | 7.7 | 8.8 | 1.14 |
| | 210 | 14.2 | 15.4 | 1.09 |
| | 220 | 33.2 | 34.4 | 1.04 |

POM/2 reaction conditions were used (cf. Table 2).

Catalyst CZZA, on the other hand, does not lose activity upon reoxidation. On the contrary, the methanol conversion slightly increases over this material. This can be ascribed to the presence of $Al_2O_3$ and $ZrO_2$ (both structural promoters) and possibly a favorable restructuring of the catalyst after reoxidation.

Over both catalysts, the product distribution at a given methanol conversion is almost identical before and after reoxidation. Both catalysts start producing $H_2$ at the expense of water with increasing temperature. $CO_2$ is the main carbon-containing product and CO levels are negligible. Over CZZA, formaldehyde and DME, which are present at low levels in the lower temperature range, diminish with increasing temperature.

### 3.7. The oxidation state of copper

Total hydrocarbon oxidation reactions are thermodynamically favored, water and $CO_2$ being the final products. Hence, partial oxidation reactions are enabled only by strict kinetic control. As these processes are strongly exothermic, heat removal and temperature control must be efficient in order to prevent the appearance of hot spots and overoxidation of the catalyst.

It is well-known that copper performs more than one catalytic function depending on its oxidation state. Copper was in the metallic state in catalyst CZ after exposure to POM/1 reaction conditions, as determined by powder X-ray diffraction measurements performed on a spent catalyst after cooling in $N_2$. However, being an ex situ technique, XRD only provides information about the bulk of the catalyst outside the reactor.

In order to gain information about the chemical state of copper on the catalyst surface, X-ray photoelectron spectra were collected for catalyst CZZA after exposure to various conditions, viz. (i) fresh after calcination in air, (ii) after reduction in 400 mbar $H_2$ at 250 °C for 1 h, and (iii) after exposure to a $O_2/CH_3OH$ mixture (1/2 M) at 60 mbar and 250 °C for 1 h. Hence, by utilizing the pretreatment chamber of the XPS instrument, pseudo in situ measurements on the catalyst's surface state after exposure to reaction conditions were possible. Nonetheless, it should be remembered

Table 4
Auger parameters ($\alpha_{Cu}$ and $\alpha_{Zn}$) and binding energies of the core electrons for catalyst CZZA determined by X-ray photoelectron spectroscopy after exposure to various conditions, i.e., (i) calcined catalyst, (ii) reduced in 400 mbar $H_2$ at 250 °C, and (iii) after exposure to 60 mbar $O_2/CH_3OH$ (1:2 M) at 250 °C

| | Auger parameters (eV) | | Binding energies (eV) | | | |
|---|---|---|---|---|---|---|
| | $\alpha_{Cu}$ | $\alpha_{Zn}$ | Cu $2p_{3/2}$ | Zn $2p_{3/2}$ | Al 2p | Zr 3d |
| Calcined | 1851.0 | 2008.4 | 934.3 | 1020.9 | 74.5 | 182.1 |
| Reduced | 1850.8 | 2008.7 | 932.4 | 1020.6 | 74.4 | 182.1 |
| *Post* reaction | 1848.8 | 2008.4 | 932.8 | 1020.9 | 74.4 | 182.2 |

that being a vacuum technique, the surface state is inevitably affected by degassing of the sample.

The binding energies of the core electrons and the modified Auger parameters ($\alpha_A$) of copper and zinc are reported in Table 4. The $Cu2p_{3/2}$ photoelectron spectra are shown in Fig. 14. In the calcined catalyst, CuO displays the characteristic peak at 934.3 eV [22,37,45,48–54]. After exposure to $H_2$, the peak shifts to 932.4 eV, indicative of $Cu^0$ formation [22,37,48,50,52–55]. The reduced sample was then exposed to $O_2/CH_3OH$. As the binding energies of $Cu^0$ and $Cu^+$ are not distinguishable on the basis of $Cu2p_{3/2}$, the modified Auger parameters ($\alpha_{Cu}$) were calculated in order to differentiate between these two species [22,48,50]. The Auger parameter of copper ($\alpha_{Cu}$) shifted from 1850.8 to 1848.8 eV upon exposure to $O_2/CH_3OH$, which is characteristic of $Cu^+$ [22,50,56].

There are no significant variations in the binding energies (or Auger parameters) of zinc, zirconium, and aluminum upon exposure to the various conditions. The characteristic features of ZnO, $ZrO_2$, and $Al_2O_3$ are observed in all cases. Some authors have proposed CuZn alloy formation under strongly reducing conditions [57], while others have suggested the existence of $CuAl_2O_4$ [37]. However, in the present investigation, none of these species were observed, unless in small quantities below detectable limits.

The surface atomic ratios of Cu/Zn, Cu/Zr, and Cu/Al in CZZA are listed in Table 5. As shown, the surface composition is strongly affected by the environment. By $H_2$ reduction and subsequent exposure to $O_2/CH_3OH$, the surface content of copper decreases quite drastically on behalf of zinc, zirconium, and aluminum.

It is difficult to draw firm conclusions based on the appearance of $Cu^+$, as the catalyst surface may oxidize during cooling after reaction and be further affected by degassing in the XPS pretreatment chamber. Reitz et al. [33] noted that upon cooling of the catalyst in the presence of a feed consisting of methanol, water, and $O_2$, there was reoxidation of copper to Cu(I), but no further oxidation to Cu(II). Nevertheless, we believe that the surface of the working catalyst contains mildly oxidized copper species, possibly coexisting with metallic copper, when producing $H_2$ by partial oxidation of methanol with $O_2$. Hence, the catalyst's POM activity may be related to its ability to form oxidized copper species

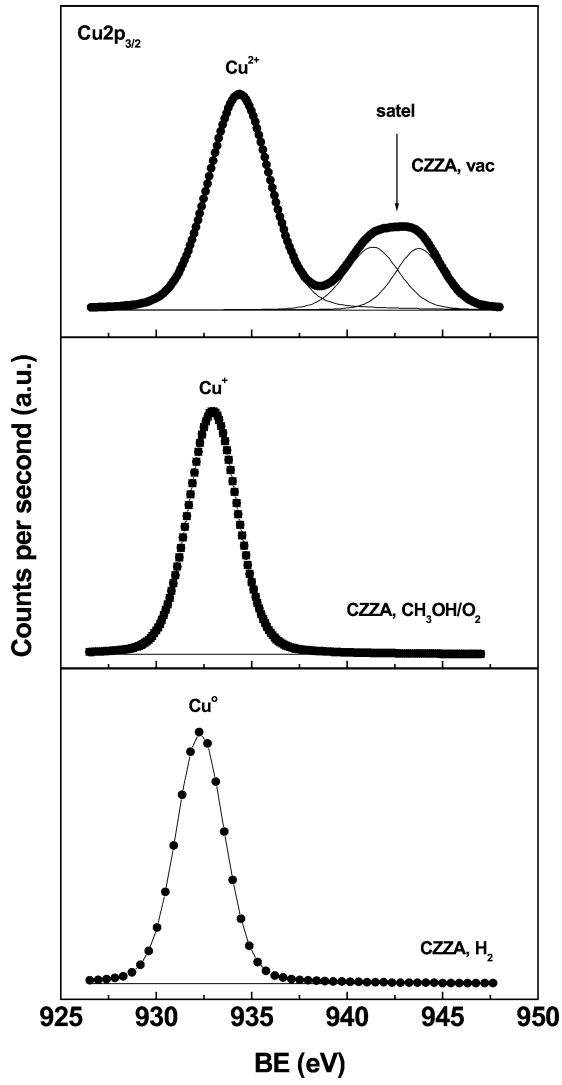


Fig. 14. $Cu2p_{3/2}$ photoelectron spectra of catalyst CZZA after calcination (top), after exposure to reaction conditions (middle), and after $H_2$ reduction (bottom).

Table 5
Surface atomic ratios of catalyst CZZA determined by X-ray photoelectron spectroscopy after exposure to various conditions, i.e., (i) calcined catalyst, (ii) reduced in 400 mbar $H_2$ at 250 °C, and (iii) after exposure to 60 mbar $O_2/CH_3OH$ (1:2 M) at 250 °C

| | Cu/Zn | Cu/Zr | Cu/Al |
|---|---|---|---|
| Calcined | 0.963 | 3.188 | 0.912 |
| Reduced | 0.633 | 2.127 | 0.667 |
| *Post* reaction | 0.374 | 1.302 | 0.438 |

on the surface. It is reasonable to assume that copper in a well-dispersed state is more easily oxidized than large copper crystallites.

In recent studies, Reitz et al. [33] and Günter et al. [58] used time-resolved XANES and in situ XAFS measurements, respectively, to demonstrate that Cu(I) oxide is a transient species in the reduction of CuO/ZnO. Hence, CuO reduction is thought to be a two-step process, in which

Cu(I) oxide forms as an intermediate prior to $Cu^0$. The latter authors further investigated the oxidation state of copper during SRM in the presence of $O_2$. They studied the bulk structure of Cu/ZnO catalysts and showed that completely reduced $Cu^0$ clusters on ZnO constitute the active bulk phase for SRM. However, they also noted that additional microstructural parameters must be considered in order to explain the catalyst's activity. By adding $O_2$ to the feed gas, a mixture of Cu(II) and Cu(I) oxides was formed accompanied by a complete loss of activity for the SRM reaction. The formation of $CO_2$ and water indicated total oxidation of methanol. It is well known that complete oxidation of copper to Cu(II) renders the catalyst inactive for $H_2$ production, instead promoting methanol combustion. The so-called "oxidative poisoning," however, was completely reversible. Although accompanied by an increase in copper crystallite size, switching back to SRM reaction conditions even lead to an increase in conversion, selectivity, and $H_2$ production rate. The enhanced activity upon repeated redox cycles was ascribed to an increasing disorder of copper particles and segregation of zinc out of the copper bulk. The increasing structural disorder (strain) was explained by the increasing Cu–ZnO interface.

In a similar study, Knop-Gericke and co-workers [59,60] characterized the active copper phase of an unsupported elemental copper catalyst under methanol oxidation conditions using in situ X-ray absorption spectroscopy (XAS). These authors report on the existence of surface oxygen species on copper, which are distinctly different from oxygen in well-defined copper oxide phases. They demonstrated that the oxidic and metastable suboxide species, respectively, affect the action mode of copper in the catalyst in different ways, hence being selective or unselective in the production of formaldehyde, which was used as the model reaction. The conversion of methanol was studied as a function of the $O_2/CH_3OH$ ratio in the feed and an activity enhancement was observed with decreasing ratios ($< 0.5$ M), coinciding with the transition from well-defined oxide phase to suboxide ($Cu_{x\geqslant 10}O$) and metallic phases. It was further shown that the suboxide phase was connected with partial oxidation activity to produce formaldehyde, rather than total oxidation. Bulk oxygen, as found in Cu(I) oxide, and surface oxygen showed negligible activity for formaldehyde production. It was further pointed out by these researchers that the suboxide phase cannot be observed under UHV conditions, as it forms only under reaction conditions.

Although partial oxidation of methanol to produce formaldehyde has many similarities with the POM process and much can be learned by studying this reaction, it should be remembered that formaldehyde production requires rapid quenching of the product gas mixture in order to avoid further decomposition of formaldehyde. As such, it is a process different from POM to produce $H_2$, in which consecutive total oxidation and steam reforming may occur, as will be discussed in the following section.

### 3.8. Reaction pathways

As noted in the preceding section, it is possible that the metallic copper surface becomes partially or completely oxidized in the presence of $O_2$ in the feed gas. $Cu^0$ oxidation reactions are thermodynamically favored:

$$Cu^0 + 0.5O_2 \rightarrow CuO, \quad \Delta H^0 = -155.2\ \text{kJ/mol}, \tag{13}$$

$$2Cu^0 + 0.5O_2 \rightarrow Cu_2O, \quad \Delta H^0 = -166.7\ \text{kJ/mol}. \tag{14}$$

As copper performs more than one catalytic function depending on its oxidation state, metallic copper being active for SRM while Cu(II) shows negligible activity for $H_2$ formation, instead producing water and $CO_2$ [22,28,30,32,33], there is a risk of catalyst deactivation when operating under incomplete $O_2$ conversions. At high methanol conversions during POM and CRM, however, all $O_2$ has been converted and the reaction mixture is reductive. Thereby, copper may again be transformed into its metallic state, which is active for $H_2$ production.

Reitz et al. [33] studied the CRM reaction over Cu/ZnO catalysts by time-resolved XANES and found that under low-conversion conditions, Cu(II) was the dominant copper species and combustion forming water and $CO_2$ the primary reaction occurring. After complete conversion of $O_2$, Cu(II) was reduced to form $Cu^0$ accompanied by the initiation of $H_2$ production through SRM. Cu(I) was observed as a transient species in the reduction of Cu(II) to $Cu^0$, but no activity was attributed to it.

Some useful information about the catalysts' surface state can be obtained by studying the activity data more closely. In Fig. 15, the methanol conversion over catalyst CZA has been plotted against the reaction temperature. As shown, the light-off temperature is similar in all three reactions. Over catalyst

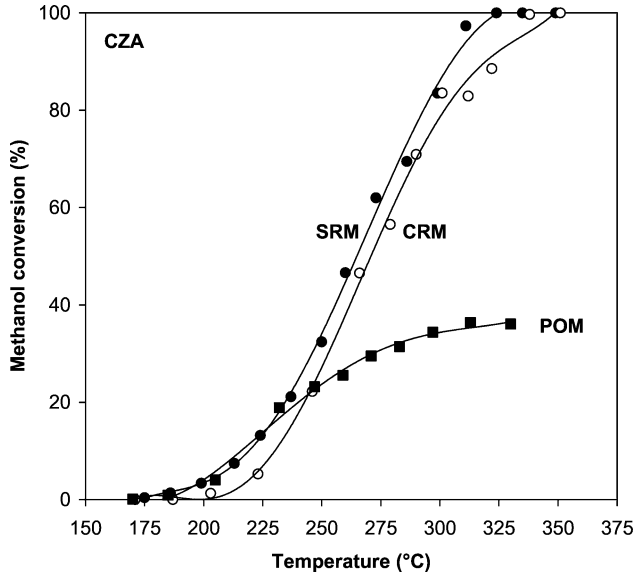


Fig. 15. Methanol conversion vs reaction temperature during (●) steam reforming, (○) combined reforming, and (■) partial oxidation of methanol over catalyst CZA ($H_2O/CH_3OH = 1.3$; $O_2/CH_3OH = 0.2$ M).

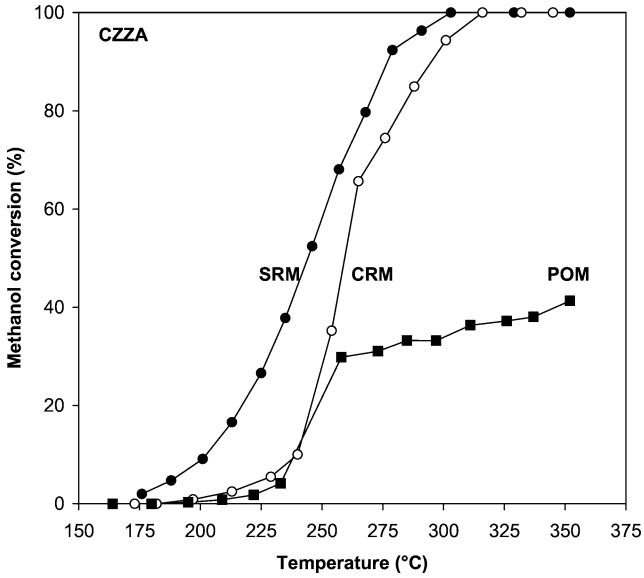


Fig. 16. Methanol conversion vs reaction temperature during (●) steam reforming, (○) combined reforming, and (■) partial oxidation of methanol over catalyst CZZA ($H_2O/CH_3OH = 1.3$; $O_2/CH_3OH = 0.2$ M).

CZZA, however, this is not observed (Fig. 16). While the SRM reaction exhibits the typical S-shaped temperature dependence of conversion, the light-off is delayed and more abrupt for the CRM and POM reactions. When all four catalysts are compared in the three processes, it is clear that they can be divided into two groups. Catalysts CZZ and CZZA exhibit a shift toward higher temperatures with respect to the initiation of $H_2$ production during CRM and POM. This is not the case for catalysts CZ and CZA. In other words, the presence of $O_2$ over $ZrO_2$-containing catalysts appears to have an inhibiting effect on methanol conversion at temperatures up to about 225 °C.

When the catalysts' properties are compared, it is evident that catalysts CZZ and CZZA are easily oxidized at low temperatures in the presence of $O_2$, as demonstrated in the TPO experiments. In addition, these catalysts contain $ZrO_2$, which is thought to exhibit synergies with copper [39–41]. They also display high stability during repeated reduction–oxidation, as shown by TPR/TPO redox cycles.

In order to investigate whether structural parameters other than the copper metal surface area exert influence on the methanol conversion activity, the turnover frequencies (TOFs) were calculated. The TOF values for methanol conversion during SRM and CRM are reported in Table 6, normalized to the number of surface copper atoms by assuming $1.46 \times 10^{19}$ copper atoms/$m^2$ [43].

Possible mass transport limitations, especially in the high-temperature regime (cf. Ref. [5]), makes it difficult to draw firm conclusions based on the comparison of calculated TOFs. For instance, differences in catalyst porosity must also be considered. Nevertheless, the TOF values are similar for all catalysts except CZZ. As the values are not independent of catalyst composition at a given temperature, it seems that properties other than copper surface area affect

Table 6
Turnover frequencies (TOFs) for methanol conversion normalized to the number of surface copper atoms during steam reforming and combined reforming of methanol

| | T | Catalyst/TOF ($s^{-1}$) | | | |
|---|---|---|---|---|---|
| | (°C) | CZ | CZA | CZZ | CZZA |
| SRM | 200 | 0.03 | 0.01 | 0.03 | 0.03 |
| | 225 | 0.05 | 0.04 | 0.10 | 0.08 |
| | 250 | 0.10 | 0.11 | 0.21 | 0.18 |
| | 275 | 0.23 | 0.20 | 0.34 | 0.27 |
| | 300 | 0.29 | 0.28 | 0.43 | 0.31 |
| | 325 | 0.34 | 0.33 | 0.46 | 0.31 |
| CRM | 200 | 0.02 | 0.004 | 0.01 | 0.003 |
| | 225 | – | 0.02 | 0.06 | – |
| | 250 | 0.16 | – | 0.19 | – |
| | 275 | 0.25 | 0.18 | 0.33 | 0.23 |
| | 300 | 0.31 | 0.28 | 0.43 | 0.30 |
| | 325 | 0.34 | 0.30 | 0.47 | 0.31 |

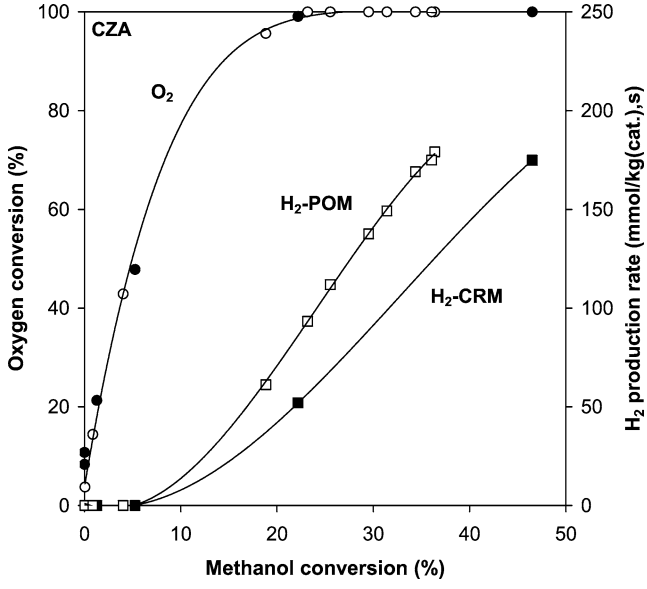


Fig. 17. $O_2$ conversion and $H_2$ production rate vs methanol conversion during steam reforming ((○) $O_2$; (□) $H_2$) and combined reforming ((●) $O_2$; (■) $H_2$) of methanol over catalyst CZA ($H_2O/CH_3OH = 1.3$; $O_2/CH_3OH = 0.2$ M).

the catalytic activity of the samples. Clearly, the *quality* of the copper surface is also a parameter of importance for the catalytic performance.

Catalyst CZZ has the highest Zr/Cu ratio of the samples studied. This feature should favor possible copper–support interactions, which may explain its higher activity for methanol conversion. In methanol synthesis and decomposition studies over $Cu/ZrO_2$ [39–41], Fisher and Bell ascribed different roles to copper and $ZrO_2$. These authors suggested that while all major reaction intermediates are located on $ZrO_2$, the role of copper is to promote hydrogen spillover.

In Fig. 17, the $O_2$ conversion and the $H_2$ production rate over catalyst CZA have been plotted against the methanol conversion during both POM and CRM. It is clear that no

$H_2$ is produced in the low-conversion region, while $O_2$ is quickly converted. $H_2$ production initiates when the $O_2$ conversion approaches completeness. The formation of water at differential $O_2$ conversions constitutes evidence of the occurrence of methanol and/or $H_2$ combustion.

Integrally, the CRM process can be seen as a combination of SRM and POM, converting methanol, water, and $O_2$ in parallel under close to autothermal conditions. However, when studying the process differentially, it is clear that $O_2$ and water are converted consecutively—$O_2$ through total oxidation and water by steam reforming. This pathway, a consecutive reaction scheme consisting of methanol combustion followed by SRM, was proposed in a previous paper from our laboratory [5] and also gains support in the literature [30,32,33,37]. An interesting feature is that water formation by combustion reactions in the low-conversion regime consumes $O_2$, hence increasing the $H_2O/CH_3OH$ ratio and suppressing CO formation by RWGS.

To further investigate the reaction pathways for the three processes, the difference in temperature between the catalyst bed and the furnace wall ($\Delta T$) was plotted against the methanol conversion for all three cases over catalyst CZ (Fig. 18). As shown, $\Delta T$ decreases almost monotonically during the endothermic SRM reaction. During both POM and CRM, there is initially a sharp increase in $\Delta T$ with methanol conversion, corresponding to the region in which methanol is combusted. The sharpest increase is observed for the POM reaction. The maxima occurring in the 20–30% methanol conversion range agree well with the points at which $O_2$ conversion reaches 100% in both reactions (see Figs. 7 and 8). The increase in $\Delta T$ due to combustion is followed by a decline as water starts to react with methanol in the SRM reaction. This provides further evidence of a reaction sequence where methanol combustion, producing water and $CO_2$, is followed by SRM to produce $H_2$.

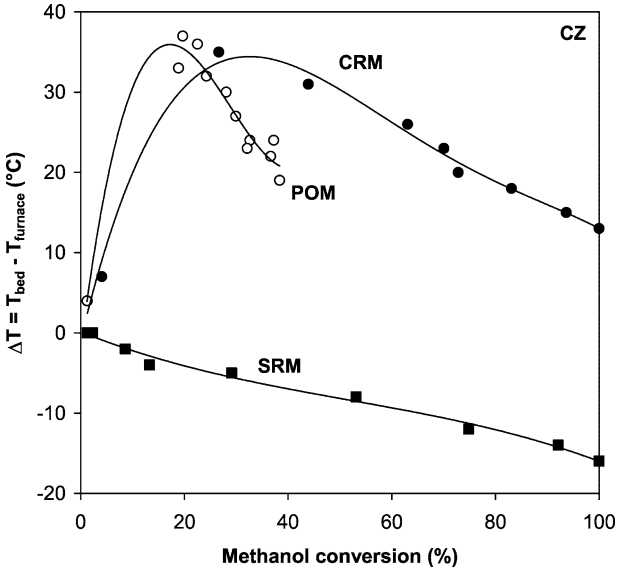


Fig. 18. The temperature difference between the catalyst bed and the furnace wall ($\Delta T$) during (■) steam reforming, (●) combined reforming, and (○) partial oxidation of methanol over catalyst CZ ($H_2O/CH_3OH = 1.3$; $O_2/CH_3OH = 0.2$ M).

During SRM and CRM, CO formation initiates over all four catalysts when the methanol conversion approaches completeness. CO appears to be a secondary product, formed by RWGS at high temperatures [18,19]. However, as discussed in a previous paper from our group, it is possible to conduct both SRM and CRM under conditions where CO concentrations are much lower than those predicted by thermodynamics [5]. The contribution from the RWGS reaction is insignificant as long as the temperature is low enough and the contact time short enough to prevent complete conversion of methanol. In the POM reaction, CO formation by methanol decomposition is unavoidable when all $O_2$ has been converted, considering the substoichiometric $O_2$ content.

## 4. Conclusions

Production of $H_2$ from methanol by steam reforming, partial oxidation, and a combination thereof was studied over a series of Cu/ZnO-based catalysts. The catalysts were derived from hydroxycarbonate precursors prepared in aqueous solution by carbonate coprecipitation of metal nitrates. Numerous activity tests were carried out in order to investigate the influence of various parameters, such as feed composition, reaction temperature, and catalyst formulation on catalytic behavior. Special attention was paid to the effect of structural and catalytic promoters ($Al_2O_3$ and $ZrO_2$).

Some clear differences between the processes were observed with respect to catalyst functionality. For instance, a catalyst that performs well during methanol steam reforming is not always suitable in the presence of $O_2$. Incorporation of $ZrO_2$ in the catalyst enhances catalytic performance in the steam reforming reaction, whereas the binary Cu/ZnO catalyst performs well during partial oxidation with early light-off and low CO levels.

The catalysts' resistance to repeated reduction–oxidation was investigated by performing TPR/TPO redox cycles. It was found that while binary Cu/ZnO exhibits poor stability, catalysts containing $ZrO_2$ and $ZrO_2/Al_2O_3$ are highly resistant to redox cycles and exhibit high stability during extended experiments on stream.

The copper dispersion in the catalyst appears to play a key role in determining the pathway for $H_2$ production. If copper is well dispersed, the metallic surface is easily oxidized in the presence of $O_2$, rendering the catalyst inactive for $H_2$ production. However, the addition of $O_2$ to the steam reforming reaction appears to be an effective way of decreasing the CO content in the product. In this way, combined steam reforming and partial oxidation of methanol can be carried out under close to autothermal conditions. However, when combining water and $O_2$ with methanol, steam reforming and partial oxidation do not occur in parallel. On the contrary, $O_2$ is completely converted at low methanol conversions,

producing water. Hence, a consecutive reaction scheme is suggested, where combustion and steam reforming occur in sequence.

## Acknowledgments

The authors are grateful for financial support from the European Union (Contract JOE3-CT97-0049). J. Agrell acknowledges funding from Ångpanneföreningens Forskningsstiftelse (Grant 01-32) and R.M. Navarro gratefully acknowledges financial support from the European Social Fund (I3P-PC2001-2 programme).

## References

[1] A.J. Appleby, F.R. Foulkes, Fuel Cell Handbook, Van Nostrand-Reinhold, New York, 1989.
[2] D.S. Watkins, in: L.J.M.J. Blomen, M.N. Mugerwa (Eds.), Fuel Cell Systems, Plenum, New York, 1993, p. 493.
[3] J. Larminie, A. Dicks, Fuel Cell Systems Explained, Wiley, New York, 2000.
[4] J. Agrell, B. Lindström, L.J. Pettersson, S.G. Järås, in: J.J. Spivey (Ed.), Catalysis—Specialist Periodical Reports, Vol. 16, Royal Soc. Chemistry, Cambridge, 2002, p. 67.
[5] J. Agrell, H. Birgersson, M. Boutonnet, J. Power Sources 106 (2002) 247.
[6] V. Pour, J. Barton, A. Benda, Coll. Czech. Chem. Commun. 40 (1975) 2923.
[7] J. Barton, V. Pour, Coll. Czech. Chem. Commun. 45 (1980) 3402.
[8] H. Kobayashi, N. Takezawa, C. Minochi, J. Catal. 69 (1981) 487.
[9] K. Takahashi, N. Takezawa, H. Kobayashi, Appl. Catal. 2 (1982) 363.
[10] E. Santacesaria, S. Carra, Appl. Catal. 5 (1983) 345.
[11] J.C. Amphlett, M.J. Evans, R.F. Mann, R.D. Weir, Can. J. Chem. Eng. 63 (1985) 605.
[12] C.J. Jiang, D.L. Trimm, M.S. Wainwright, N.W. Cant, Appl. Catal. A 93 (1993) 245.
[13] C.J. Jiang, D.L. Trimm, M.S. Wainwright, N.W. Cant, Appl. Catal. A 97 (1993) 145.
[14] J.C. Amphlett, K.A.M. Creber, J.M. Davis, R.F. Mann, B.A. Peppley, D.M. Stokes, Int. J. Hydrogen Energy 19 (1994) 131.
[15] J.C. Amphlett, K.A.M. Creber, R.F. Mann, B.A. Peppley, Int. J. Hydrogen Energy 21 (1996) 673.
[16] B.A. Peppley, J.C. Amphlett, L.M. Kearns, R.F. Mann, Appl. Catal. A 179 (1999) 21.
[17] B.A. Peppley, J.C. Amphlett, L.M. Kearns, R.F. Mann, Appl. Catal. A 179 (1999) 31.
[18] J.P. Breen, J.R.H. Ross, Catal. Today 51 (1999) 521.
[19] J.P. Breen, F.C. Meunier, J.R.H. Ross, Chem. Commun. 22 (1999) 2247.
[20] P.J. de Wild, M.J.F.M. Verhaak, Catal. Today 60 (2000) 3.
[21] B. Lindström, L.J. Pettersson, Int. J. Hydrogen Energy 26 (2001) 923.
[22] L. Alejo, R. Lago, M.A. Peña, J.L.G. Fierro, Appl. Catal. A 162 (1997) 281.
[23] S. Velu, K. Suzuki, T. Osaki, Catal. Lett. 62 (1999) 159.
[24] J. Agrell, K. Hasselbo, K. Jansson, S.G. Järås, M. Boutonnet, Appl. Catal. A 211 (2001) 239.
[25] T.-J. Huang, S.-W. Wang, Appl. Catal. 24 (1986) 287.
[26] T.-J. Huang, S.-L. Chren, Appl. Catal. 40 (1988) 43.
[27] S. Velu, K. Suzuki, T. Osaki, Chem. Commun. 23 (1999) 2341.
[28] J.L.G. Fierro, Stud. Surf. Sci. Catal. 130 (2000) 177.
[29] E. Newson, P. Mizsey, T. Truong, P. Hottinger, Stud. Surf. Sci. Catal. 130 (2000) 695.
[30] T.L. Reitz, S. Ahmed, M. Krumpelt, R. Kumar, H.H. Kung, Stud. Surf. Sci. Catal. 130 (2000) 3645.
[31] S. Velu, K. Suzuki, M. Okazaki, M.P. Kapoor, T. Osaki, F. Ohashi, J. Catal. 194 (2000) 373.
[32] T.L. Reitz, S. Ahmed, M. Krumpelt, R. Kumar, H.H. Kung, J. Mol. Catal. A 162 (2000) 275.
[33] T.L. Reitz, P.L. Lee, K.F. Czaplewski, J.C. Lang, K.E. Popp, H.H. Kung, J. Catal. 199 (2001) 193.
[34] K. Geissler, E. Newson, F. Vogel, T.-B. Truong, P. Hottinger, A. Wokaun, Phys. Chem. Chem. Phys. 3 (2001) 289.
[35] P. Mizsey, E. Newson, T.-B. Truong, P. Hottinger, Appl. Catal. A 213 (2001) 233.
[36] S. Velu, K. Suzuki, M.P. Kapoor, F. Ohashi, T. Osaki, Appl. Catal. A 213 (2001) 47.
[37] S. Murcia-Mascarós, R.M. Navarro, L. Gómez-Sainero, U. Costantino, M. Nocchetti, J.L.G. Fierro, J. Catal. 198 (2001) 338.
[38] J.-P. Shen, C. Song, Catal. Today 77 (2002) 89.
[39] I.A. Fisher, A.T. Bell, J. Catal. 172 (1997) 222.
[40] I.A. Fisher, A.T. Bell, J. Catal. 178 (1998) 153.
[41] I.A. Fisher, A.T. Bell, J. Catal. 184 (1999) 357.
[42] G.C. Chinchen, C.M. Hay, H.D. Vandervell, K.C. Waugh, J. Catal. 103 (1987) 79.
[43] R.M. Dell, F.S. Stone, P.F. Tiley, Trans. Faraday Soc. 49 (1953) 195.
[44] J.-L. Li, T. Inui, Appl. Catal. A 137 (1996) 105.
[45] Y. Okamoto, K. Fukino, T. Imanaka, S. Teranishi, J. Phys. Chem. 87 (1983) 3740.
[46] M.S. Spencer, Nature 323 (1986) 685.
[47] M.V. Twigg, M.S. Spencer, Appl. Catal. A 212 (2001) 161.
[48] W.-L. Dai, Q. Sun, J.-F. Deng, D. Wu, Y.-H. Sun, Appl. Surf. Sci. 177 (2001) 172.
[49] A. Wolberg, J.L. Ogilvie, J.F. Roth, J. Catal. 19 (1970) 86.
[50] C.D. Wagner, L.H. Gale, R.H. Raymond, Anal. Chem. 51 (1979) 466.
[51] G. Ertl, R. Hierl, R. Knözinger, N. Thiele, H.P. Urbach, Appl. Surf. Sci. 5 (1980) 49.
[52] B.R. Strohmeier, D.E. Leyden, R.S. Field, D.H. Hercules, J. Catal. 94 (1985) 514.
[53] B. Peplinski, W.E.S. Unger, I. Grohmann, Appl. Surf. Sci. 62 (1992) 115.
[54] G.G. Jernigan, G.A. Somorjai, J. Catal. 147 (1994) 567.
[55] Y. Okamoto, K. Fukino, T. Imanaka, S. Teranishi, J. Phys. Chem. 87 (1983) 3747.
[56] T.H. Fleish, R.L. Mieville, J. Catal. 90 (1984) 165.
[57] J.-D. Grunwaldt, A.M. Molenbroek, N.-Y. Topsøe, H. Topsøe, B.S. Clausen, J. Catal. 194 (2000) 452.
[58] M.M. Günter, T. Ressler, R.E. Jentoft, B. Bems, J. Catal. 203 (2001) 133.
[59] T. Schedel-Niedrig, M. Hävecker, A. Knop-Gericke, R. Schlögl, Phys. Chem. Chem. Phys. 2 (2000) 3473.
[60] A. Knop-Gericke, M. Hävecker, T. Schedel-Niedrig, R. Schlögl, Top. Catal. 15 (2001) 27.